Using ambient noise correlation at the CaMI Field Research Station, Newell County, Alberta, Canada

Marie Macquet and Don C. Lawton

ABSTRACT

At the CaMI Field Research Station we recorded several weeks of continuous surface and borehole seismic data to study the feasibility of using ambient noise correlation (also called interferometry) to monitor CO_2 injection. We focus here on the October 2017 dataset (prior to injection), composed of 14 days of continuously recorded data at the 98 stations of a 3C-3D permanent array (receiver grid of 10 m x 10 m). We use a standard processing (mean and trend removal, 1bit, spectral whitening) and compute the 14 daily ZZ-correlations for the 4753 pairs of stations to reconstruct the Green's function between them. Daily correlations show stable waveform for the baseline dataset with a good correlation coefficient between the reference and the daily correlations. Variations in the elastic parameters of the subsurface due to CO_2 injection will directly affect the reconstructed Green's function, and passive recording should allow us to detect the induced change of the medium. Interferometry can also be used as a tomographic tool through the analysis of the dispersion curve of the reconstructed Green's functions. We compute the dispersion curves for few couples of stations. A detailed analysis will be undertaken to determine why some periods show outlier values, but the group velocities obtained are similar to those found in literature.

INTRODUCTION

Reducing GHG emissions and climate impacts is a major global challenge. CO_2 capture, utilization and storage, with an emphasis on post-combustion capture and storage in geological media is a successful and important method for achieving international commitments (Mac Dowell et al., 2017). Several large-scale projects demonstrate the potential of capture and storage solutions, such as Aquistore in Canada (Rostron et al., 2014), Sleipner in Norway (Arts et al., 2008) or Ketzin in Germany (Bergmann et al., 2013). The development of the plume as well as the integrity of the cap-rock are highly monitored during the life cycle of a CO_2 storage site. We proposed here to use the continuous seismic data as an addition tool to monitor the gas injection. Passive data can be used to detect very weak events due to injection (e.g Olivier et al. (2018)) but can also be used for ambient noise tomography purposes.

In this study, we first give an overview of the CaMI Field Research Station and its instrumentation. We then present the ambient noise correlation method as well as the dataset used. Some preliminary results are then presented and discussed.

CAMI.FRS

The Containment and Monitoring Institute (CaMI) of CMC Research Institutes Inc., in collaboration with the University of Calgary, has developed a comprehensive Field Research Station (FRS) in southern Alberta, Canada, located 200km SE of Calgary (Figure 1). The purpose of CaMI.FRS is to develop new technologies to prevent and monitor early leakages of a deepest, large-scale CO_2 reservoir rather than focusing on the volume of CO_2 stored the site. To simulate a leakage, a small amount of CO_2 (around 400 t/year over 5 years) is being injected into a shallow target reservoir at a depth of 300 m (Figure 1). Phase 2 of the project will be a deeper injection in the Medicine Hat Sandstones formation (500m depth).

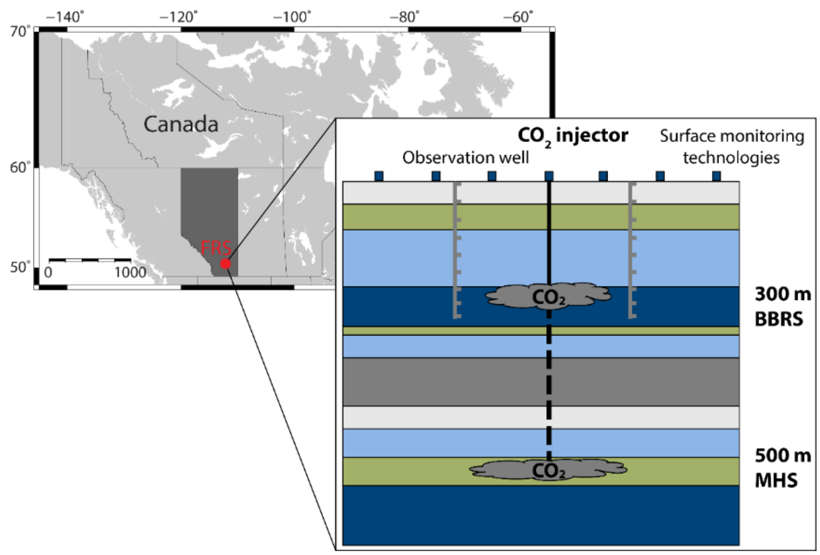

FIG. 1. Location and schematic of the CaMI Field Research Station near Brooks, AB (Canada). BBRS: Basal Belly River Sandstones. MHS: Medicine Hat Sandstones.

Due to the low injection mass and shallow target, FRS provides an ideal site to develop and improve multidisciplinary CO_2 monitoring technologies with particular focus on CO_2 detection thresholds.

To detect and monitor the injected CO_2, different geochemical and geophysical instruments are in place on the field (Lawton et al., 2015b). So far, they are used to characterize the subsurface and will be used as baseline for the monitoring studies. A non-exhaustive list of geophysical instruments on CaMI.FRS includes:

- a Digital Acoustic Sensing (DAS) optical fiber permanently installed (for example Gordon and Lawton (2017), Hall et al. (2017), Lawton et al. (2017) and Gordon and Lawton (2018));
- VSP experiments with downhole geophones (for example Hall et al. (2015), Gordon et al. (2016) and Hall et al. (2018));
- surface seismic survey (for example Isaac and Lawton (2015) and Isaac and Lawton (2017));
- a permanent array of 10x10 geophones (10m spacing, buried at 1m depth) with permanent sources (for example Lawton et al. (2015a), Spackman and Lawton (2017) and Spackman and Lawton (2018)).

GENERAL CONSIDERATIONS ABOUT AMBIENT NOISE CORRELATION

Theory

Apart from the ballistic waves generated by punctual sources (such as earthquake or man-made sources), seismic station also records the seismic ambient noise. This noise is generated by numerous phenomenons depending on the considered frequency range:

- High frequencies ($> 1Hz$) are due to anthropic noise such as roads, factories...
- $\approx$ Hz is due to local meteorological events such as rain or wind.
- Low frequencies ($< 1Hz$) are due to global meteorological events and oceans.

Ambient noise correlation studies are based on the principle that you can reconstruct the Green's function between two stations by correlation the continuous signal recorded at these two stations (Figure 2). To be accurate, only an approximation of the Green's function can be reconstructed.

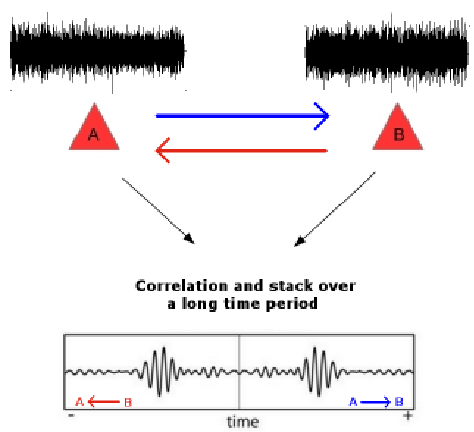

FIG. 2. Illustration of the principle of noise correlation.

Indeed, the Green's function is the transfer function of a medium or in other words is the response of the medium to a Dirac (by definition an impulse signal with an infinite frequency range - $\delta(x)\delta(t)$). Only by the fact that the seismic instruments are limited in frequency range can explained why only a partial reconstruction of the Green's function can be obtained. The non-perfect homogeneous distribution of the noise sources can also have an impact on the reconstruction of the Green's function.

Campillo and Paul (2003) were the first to apply the theory to real data. By correlating the seismic coda for different pairs of stations in California, they retrieved the approximation of the Green's function. The coda of earthquakes being an in-between signal of the impulsive response due to an EQ and the noise, the next step was taken by Shapiro and Campillo (2004) by using only ambient noise. By showing the possibility to reconstruct the Green's function from only ambient noise correlation, this pioneer paper opened a whole new field in seismology. Next step was taken quickly by Shapiro et al. (2005) who present the first surface wave tomography obtained using ambient noise correlation. Next logical step was to inverse the dispersion curves obtained from the reconstructed surface waves to S-waves velocity model of the medium (e. g. Stehly et al. (2009)).

Ambient noise correlation is now widely used for crustal tomography purposes (Macquet et al. (2014) among a lot of others).

Monitoring using ambient noise correlation

The result of the correlation depends of the properties of the medium between the two stations. If you change the elastic properties of the medium, the result of the correlation will also change (Figure 3).

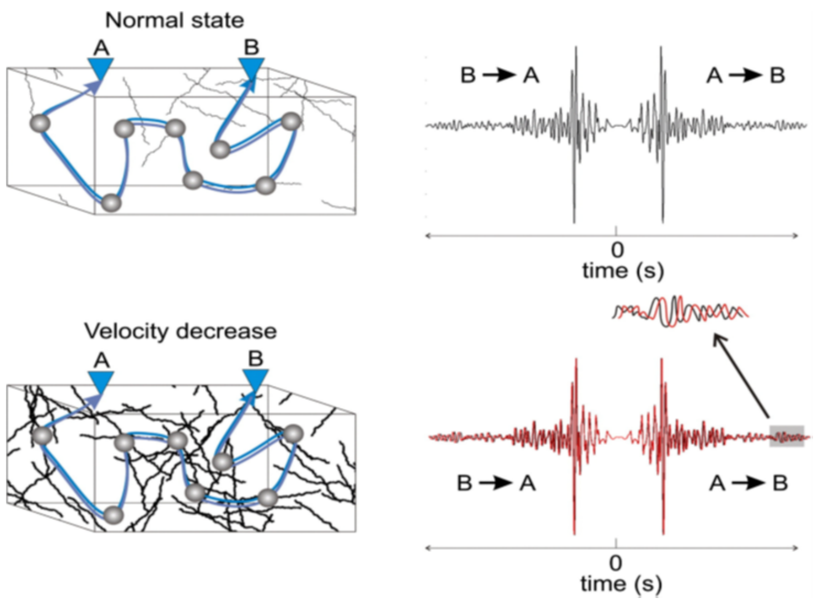

FIG. 3. Sketch representing the principle of seismic velocity change detection from travel time perturbations in the coda of noise correlation functions. Right: Corresponding correlation. In black, for the normal state, in red, with decreasing in the medium velocity. Figure 3 in Brenguier et al. (2016)

From this affirmation emerged the idea of using the ambient noise correlation (also called interferometry) for monitoring purposes. For example, this method was applied on volcanoes (e.g. Figure 4.b, Duputel et al. (2009)), on geothermal site (Figure 4.a, Obermann et al. (2015)) and a feasibility studies were done the Ketzin CO_2 storage field (Delatre and Manceau (2013), Boullenger et al. (2015)). The main challenge on that last application is the few changes of the medium due to gas injection, which make it difficult to detect by interferometry. This is particularly the case on the Field Research Station.

a) b)

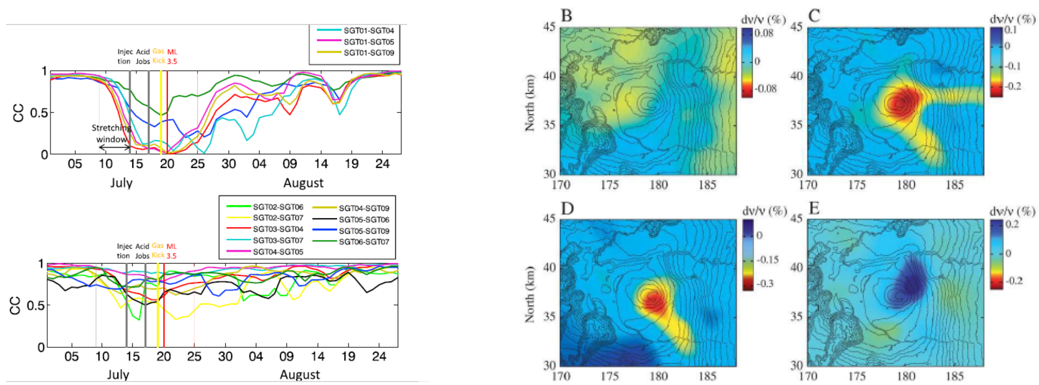

FIG. 4. a) Observed waveform coherence (CC) for the indicated station pairs. Top: close to the injections. Bottom: further away from the injections. The vertical lines in the CC plots mark the injection tests, the gas kick and the ML3.5 earthquake. From Obermann et al. (2015). b) Regionalization of temporal changes. dv/v are obtained using the stretching technique. (B), period without eruption or cyclones. (C), July 2006 pre-eruptive period. (D), August 2006 pre-eruptive phase. (E), August 2006 post-eruptive period. From Duputel et al. (2009).

APPLICATION TO THE CAMI FIELD RESEARCH STATION

Datasets

Different configurations of survey were used to record continuous ambient noise at the FRS over the last one year and a half.

The dataset used in the study was acquired in from October 11^{th} 2017 to October 25^{th} 2017 ($\approx$ 360 hours) on 98 instruments (Figure 5.a) leading to 4753 possible correlations (and 98 autocorrelations).

a) b)

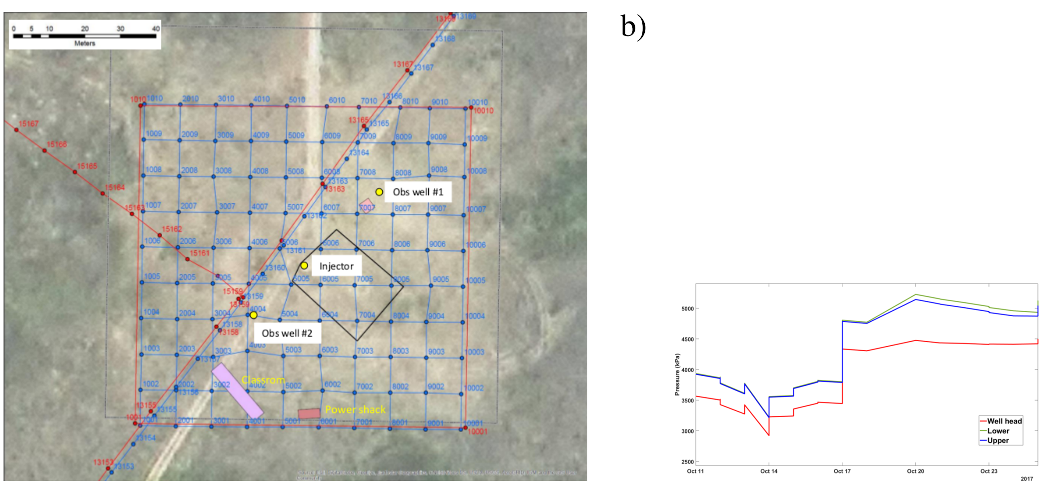

FIG. 5. a) Permanent array installed at the Field Research Station. Note that 5002 and 6002 were not used. b) Pressure profiles for three gauges along the injection well from October 11^{th} 2017 to October 25^{th} 2017. Lower gauge is at 280m depth, upper gauge at 270m depth.

During this period, very small amount of gas was injected leading to small of pressure in the medium (Figure 5.b). The three last days of the continuous recording period were busy days on the field as active seismic survey was conducted.

Raw traces

No instrumental response was removed because same instruments were used for the 98 stations. Usual preprocessing of removing the mean and the trend was done. We show in this section some examples of continuous data recorded in October 2017.

Noise

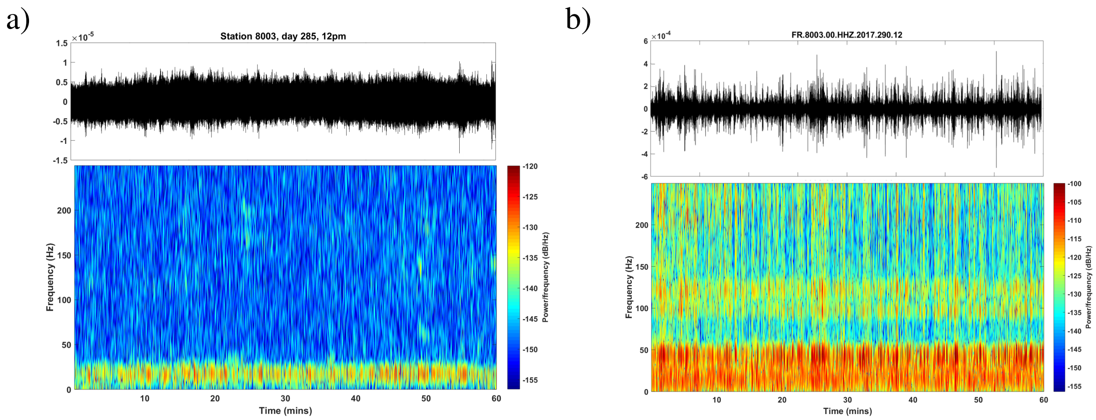

FIG. 6. Top: Raw trace. Bottom: Spectrogram. a) 1 hour of noise, day 285 (Thursday 12th October 2017), 12PM UTC. b)1 hour of noise, day 290 (Thursday 17th October 2017), 12PM UTC.

Figure 6 shows 2 hours of continuous signal, both for the same stations and at 12PM but for different days. Figure 6.a shows a quiet day, with a maximum frequency content between 1 and 30Hz. Figure 6.b shows a busier signal (top) with higher frequencies. Spectrogram is more complex with a maximum energy is between 1 and 50Hz, and a second band of maximum energy between 100 and 140Hz.

Vibe shot

Figure 7.a shows 1 hour of continuous signal during field work where the Vibroseis truck was used. We can notice on the top figure high amplitudes in the temporal signal. High frequencies content can also be observed on the bottom figure. Figure 7.b shows a zoom of 5 minutes of field work. We can see 4 sweeps signal on the top figure. They are traduced by high frequencies content on the bottom figure. The frequency content is not constant with time and shift towards high frequencies over a 16s period. It is the signature of the sweep used during that field work (10 - 150 Hz over 16 seconds).

Others punctual signal

In addition to pure noise and sweeps due to field work, we can also observe punctual events on the continuous signal. Figures 8 and 9 show two type of events we can see repeatedly over the recorded period.

Note that those kinds of spectral signatures were observed a numerous time over the 14 days periods. They are also correlated between stations and can consequently having a negative influence on the reconstruction of the Green's function.

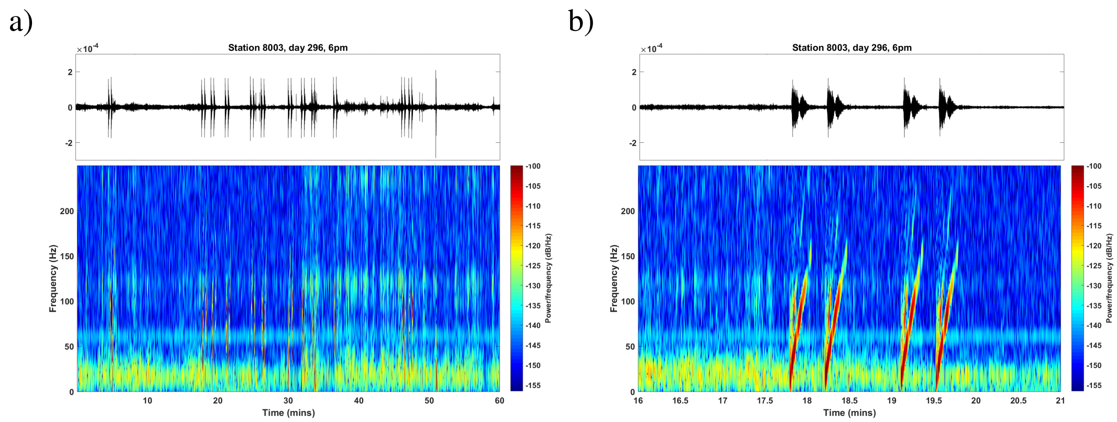

FIG. 7. Top: Raw trace. Bottom: Spectrogram. a) 1 hour of field work, day 296 (Monday October 23th 2017), 6PM UTC. b) Zoom of 5 minutes.

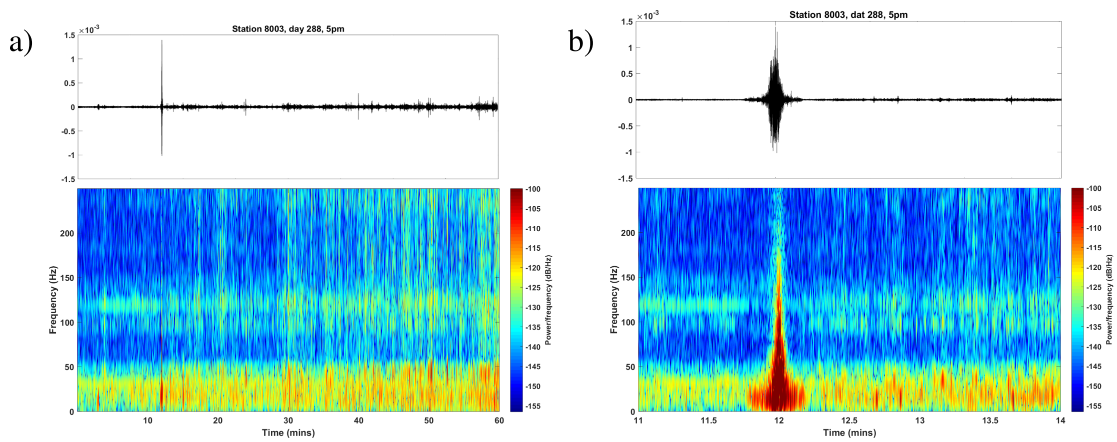

FIG. 8. Top: Raw trace. Bottom: Spectrogram. a) 1 hour of continuous signal, day 288 (Sunday October 15th 2017), 5PM UTC. b) Zoom of 3 minutes.

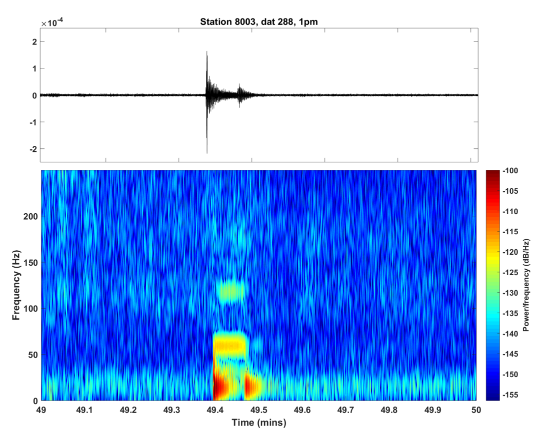

FIG. 9. Top: Raw trace. Bottom: Spectrogram. 1 minute of continuous signal, day 288 (Sunday October 15th 2017), 1:49PM UTC.

Processing

The following processing is applied to remove the effect of punctual events that we can observe in the continuous signal (see section raw traces). Indeed, those events are strongly correlated between stations (see Figure 10) and so affect the results of the reconstructed Green's function.

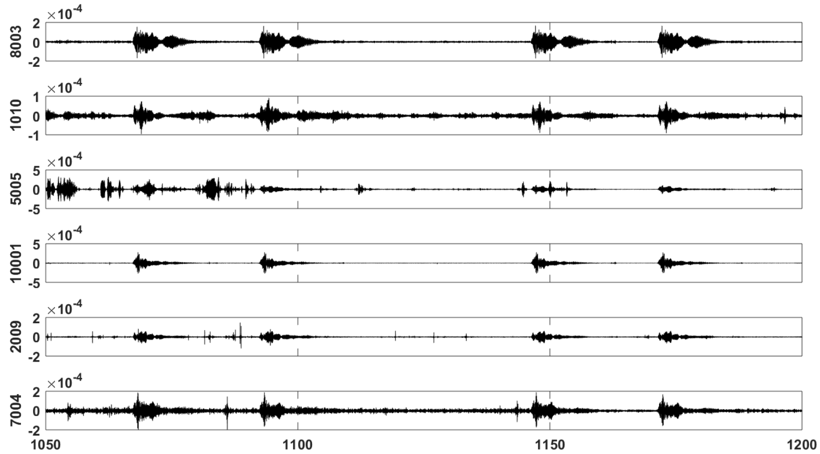

FIG. 10. Signal for 6 different stations showing sweeps.

The raw signal is first down sampled from 1000 to 200Hz to reduce the computing time. The processing is then done in the two domains:

- time-domain normalization. The most used is the 1bit normalization, which consist to put all the negative values of the signal to -1 and all the positive to 1. Other common used time normalization is the clipping, where the traces are clipped to x time the RMS of the trace. These two time-normalization will avoid having strong amplitudes in the signal due to punctual events. Another type of temporal normalization is to remove the windows containing a punctual event using automated event detection. An overview of the temporal normalization and their effect on the reconstructed Green's function quality can be found in Bensen et al. (2007), Figure 3. Note that it was proven than there is no universal processing. The same process can work well on a study but poorly on another. The optimal processing will be function of the array, the goal of the study...

- frequency-domain normalization. The spectral whitening is used for this step. It consists to flatten the frequency spectrum of a signal, to reduce the frequency content of punctual event. This step is also particularly important when using broadband stations and low frequencies (<1Hz), where the microseism peaks can be observed.

Figure 11.a and b shows and illustration of the processing on 30 seconds of noise. Spectrogram of the raw signal already shows a nice flat spectrum over time. 1bit processing is illustrated on Figure 11.a, middle row. We can notice that this temporal processing may act like a filer as some high frequencies are sometimes introduced (for example at 0.4397 on Figure 11.b, middle row). Last step of the processing, the spectral whitening (here between 1-50Hz for illustration) re-flatten the spectra of the signal (Figure **??**.b, bottom row).

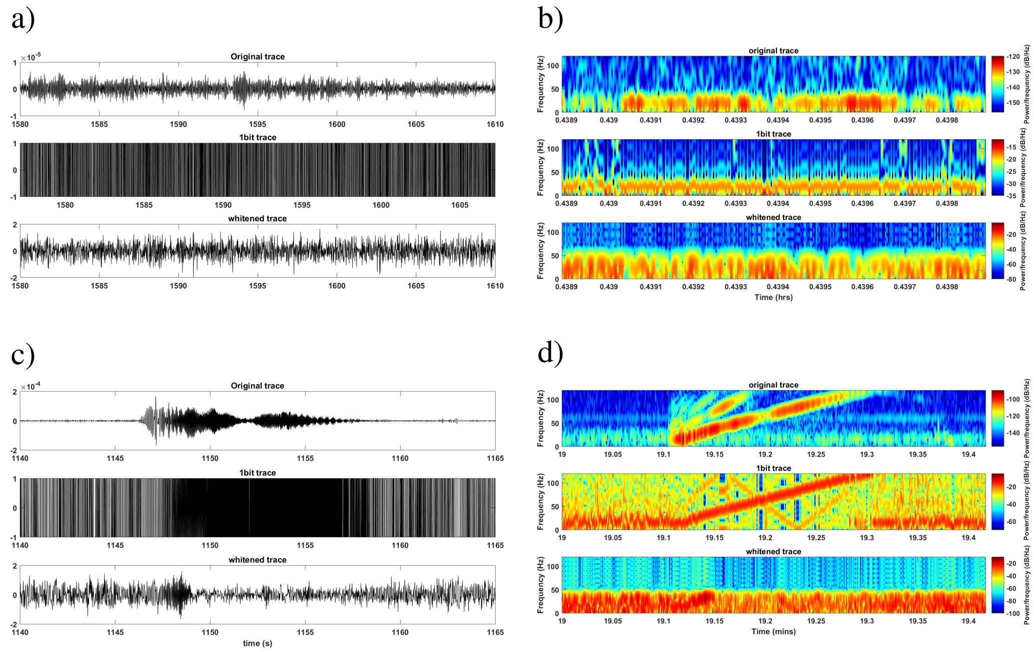

FIG. 11. a) 20s of noise, top: raw trace. Middle: 1bit processing. Bottom: Spectral whitening. b) Corresponding spectrogram. d) Corresponding spectrogram. c) 25s of Vibe signal, top: raw trace. Middle: 1bit processing. Bottom: Spectral whitening. d) Corresponding spectrogram.

Figure 11.c and d shows the effects of the processing on 30s of signal containing one shot of vibe. As explained in previous section, we clearly see the effect of the vibe shot on the raw spectrogram (Fig. 11.d, top row). 1bit processing (middle rows) clearly reduces the high amplitudes due to the shot. However, the spectrogram (Fig. 11.d middle row) still clearly shows the high frequencies content due to the shot (also observed on the signal on Figure 11.c, middle row). Spectral whitening erases the high frequencies and flattened the spectrum as shown on Figure 11.d, bottom row.

Results - Distance plot

We use the Python open source code developed by Lecocq et al. (2014) to process the continuous data as explained in the previous section and compute the correlations. Spectral whitening was done in the [0.5 - 30] Hz frequency band.

Figure 12 shows the ZZ correlations with a SNR > 14. SNR is computed as the ratio of the rms of the window containing the emerged Rayleigh waves over the rms of a window of noise. We clearly see non-symmetry in the correlations which indicate a non-homogenous distribution of the sources of noise. However, Hadziioannou et al. (2009) show that the prefect reconstruction of the Green's function is not a necessary condition to use ambient noise correlation for monitoring purposes.

Figure 13 shows the stacked correlations having a SNR superior to 12. Red line corresponds to the velocity 240m.s^{-1}, roughly corresponding the maximum energy in the correlation.

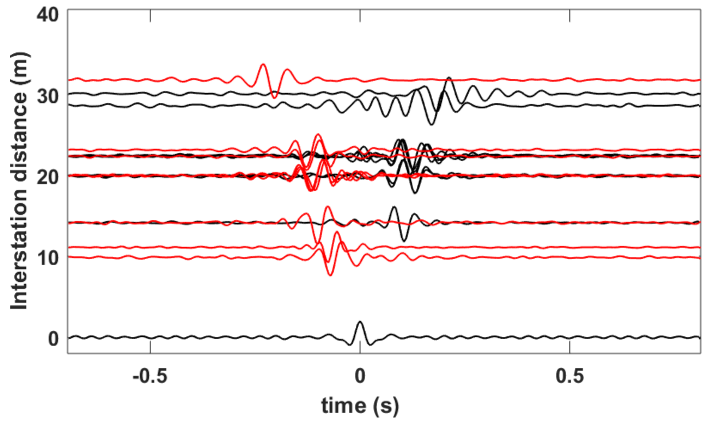

FIG. 12. Empirical Green's function as function of interstation distance (for correlations with SNR>14). Red: Strong amplitude observed on acausal part of the correlation. Black: Strong amplitude observed on the causal part of the correlation.

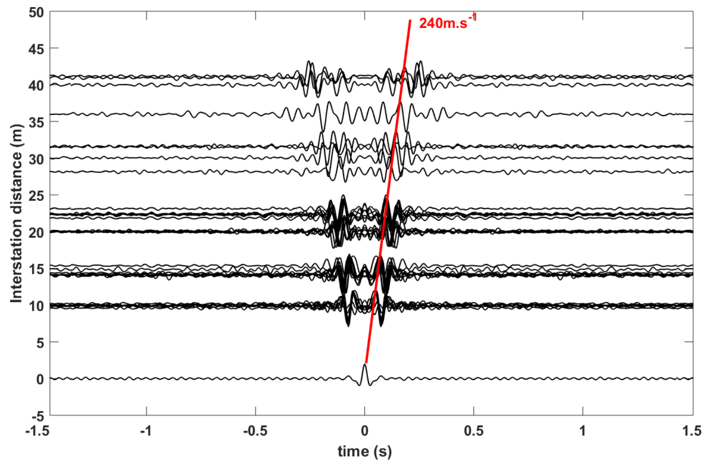

FIG. 13. Empirical Green's function as function of interstation distance (for correlations with SNR > 12). Causal and acausal parts are stacked.

DISPERSION CURVES

Surface waves are the dominant part of the reconstruction of the Green's function. They are dispersive waves and can be characterized by their group or phase velocity. We use frequency-time analysis (FTAN, Levshin et al. (1989)) to compute the group velocity dispersion curves of the stacked correlation for selected pairs of stations. Figure 14 shows the spectrogram and picked dispersion curves for 3 pairs of stations, with an interstation of 56.6, 80 and 130m. Note that the spectral whitening being done on the [0.5-30] Hz frequency band, values outside that band are not relevant. The value for group velocities are coherent with the ones found in Storke et al. (2018) or Mordret et al. (2014). Dispersion curves of surface waves are sensitive primary to the S-wave velocity of the subsurface, but also to the P-wave velocity and the density. Later on, these dispersion curves will be inverted to have elastic parameters model (using for example Herrmann (2013) and will be compared with the ones obtained from other methods.

a)

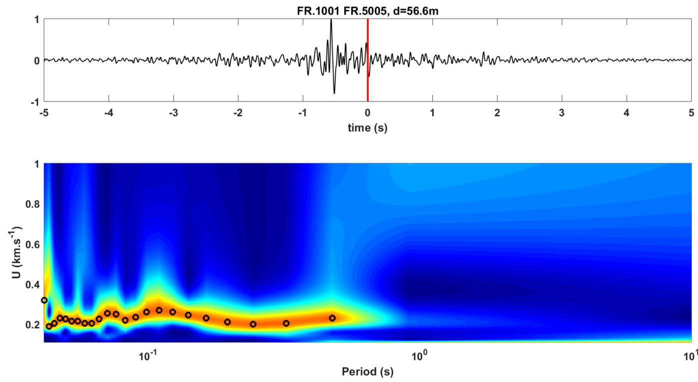

b)

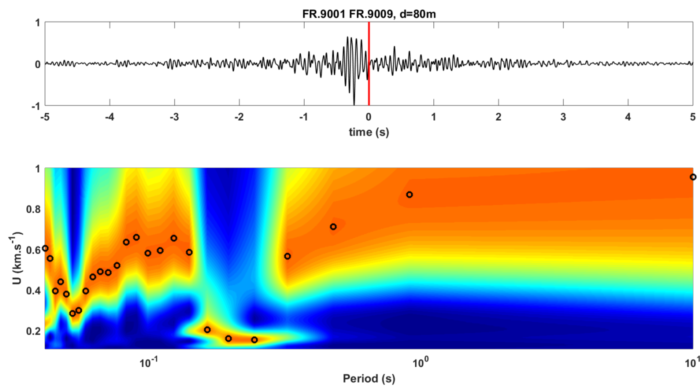

c)

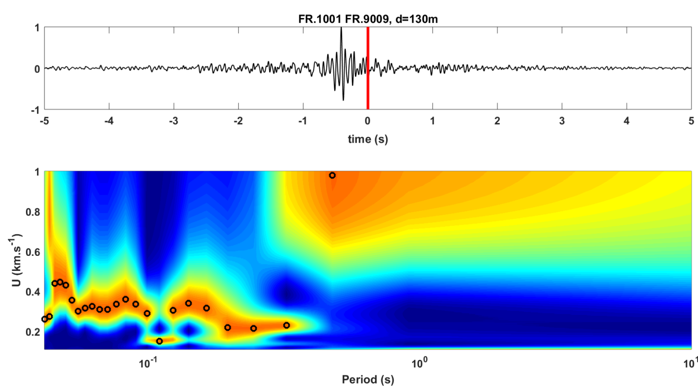

FIG. 14. Correlations and corresponding spectrogram. Maximum amplitudes picked are shown as black circles and correspond to the group velocity dispersion curve. a) Distance interstation of 56.6m. b) Distance interstation of 80m. c) Distance interstation of 130m.

Results - Correlation Stability

Application of using interferometry for monitoring purposes requires a good stability in the correlations. The October 2017 dataset can be considered as baseline as very few amounts on CO_2 was injected during this period (Figure 5.b). In order to be able to detect small changes, we need to be sure that the baseline correlations remain similar with time. Figure 15 shows the reference correlation as the stack of the 14 days period on the top. Middle panel shows the 14 daily correlations. We can already see the stability in the daily correlations. Right panel shows the correlation coefficient between the reference correlation and the daily correlation (coefficient being 1 when signals are perfectly correlated).

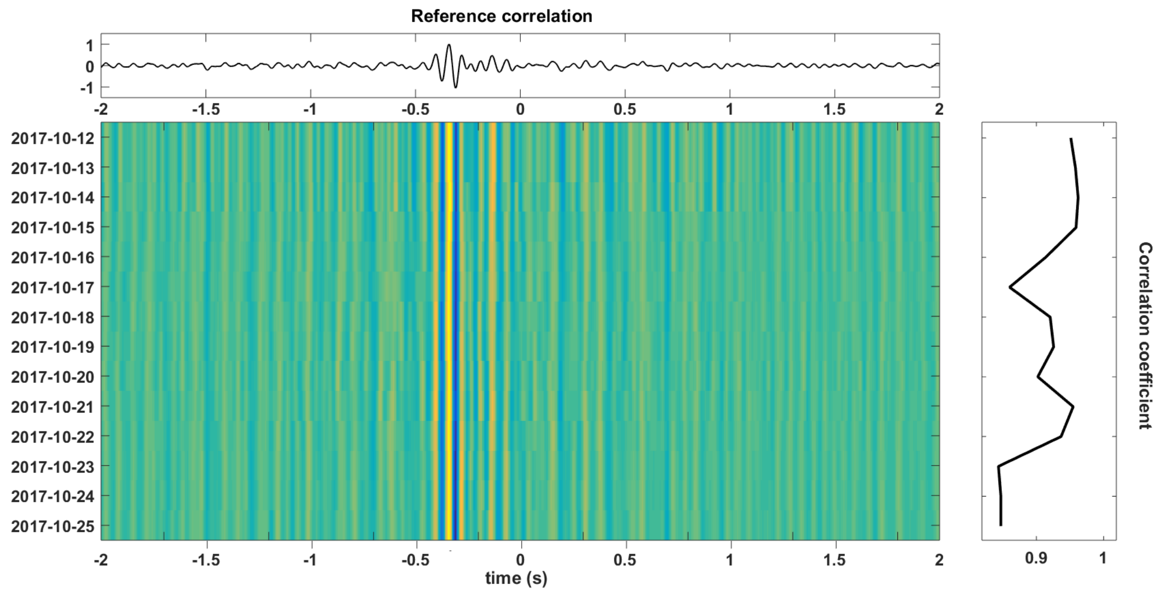

FIG. 15. Stability of the correlation between the station 1009 and 9001 (80m apart). Top: Reference correlation (14 days stacked). Middle panel: Interferogram of the daily correlations. Right: Correlation coefficient between the reference correlation and the daily ones.

In the MSNoise package, Lecocq et al. (2014) implement the Moving-Window Cross Spectrum analysis (MWCS, first introduced by Ratdomopurbo and Poupinet (1995)). For a detailed theory, lectors can refer to Clarke et al. (2011). Once $\delta t/t$ is obtained, $\delta v/v$ can be easily computed as shown in Ratdomopurbo and Poupinet (1995). We test the method on a subset of 5 stations (4 in the corners of an 80m size square, 1 in the center). Results are shown on Figure 16.a for two pairs of stations, as well as associated errors. Figure 16.a also shows the average $\delta v/v$ for the 10 possible station pairs. The 5 different subfigures show the velocity variations as a function of number of stacked days to obtain the considered correlation (here 1,2,3,4 and 5 days). For a better comparison, the 5 mean curves are also plotted on Figure 16.b. As expected, the more days you use for the current correlation, the less velocity variations you observed. That can be explained by the simple fact that the velocity variations you may expected at small time-scale are averaged and so smoothed over a longer period of time. The "high" amplitudes tend to disappear when a higher number of days is stacked.

The top plot of Figure 16.a shows the velocity variation for the daily correlations. The maximum of the average variation is 0.025% (green curve). However, we can see that the pairs of stations can show higher velocity variation (up to 0.07% for the FR.1001-FR.1009 stations, orange curves).

Even small (± 0.01%), the mean velocity variations on the Figure 16 seems to show a global decreasing of velocity over time. Several authors (for example Mainsant et al. (2012), Gassenmeier et al. (2014), citehillersetal2015) showed that natural phenomena such as wind, groundwater level, or temperature may have a strong influence on the results of interferometry. We expect such small on the elastic properties due to CO_2 injection at the Field Research Station that a careful study of the results needs to be done to proper understand the meaning of our results.

a)

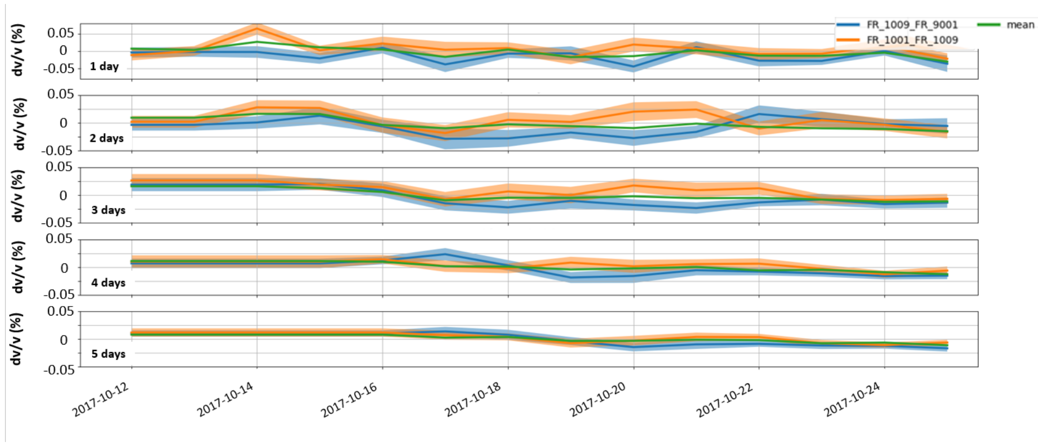

b)

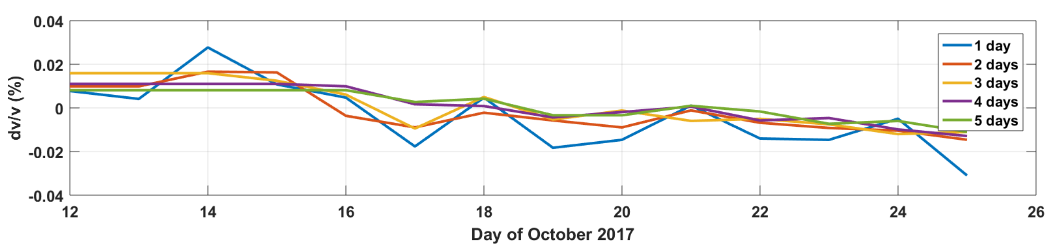

FIG. 16. a) $\delta v/v$ obtained for two pairs of stations (orange and blue) and mean $\delta v/v$ for the subset of 5 stations (green). Note the amplitude of used scale is higher for 1 day (top plot, ± 0.08% than for the 4 other plots (± 0.05%). b) Mean velocity variations for different number of stacked days.

FUTURE WORK

As explained in the previous section, further work needs to be done on the October 2017 dataset. It is including the inversion of the dispersion curves to elastic models and a more comprehensive analyze of the results in the velocity changes observed on correlations.

We recorded new continuous data in February 2018 by adding to the 3D path (Fig. 5.a) 103 geophones along the 2D trench (1km long, 10m spacing) to get a larger array aperture. This brings the total number of geophones to 201, for a continuous recording time of 25 days. This dataset is also considered as baseline as very few amounts of CO_2 was injected between October 2017 and February 2018. However, environment conditions were different with freezing temperatures and snow falls during the second experiment.

Analyzing the two datasets will allow to determine the possible effect of environmental conditions on the reconstruction of the Green's function and the study of velocity variations.

Smaller experiments were conduct in October and November 2018 (1 week of continuous data on 10 geophones deployed close to the injection well). During this period, "high" pressure injection tests were conducted to better understand the process leading to the temperature drops observed in some conditions ($\approx$ -0.75°C when pressure in the gauges reaches 4.7MPa). One of the explanations is the creation of thermal fracturing and the objective is to see if we can detect this phenomenon on the recording continuous seismic signal using for example match-field processing (Olivier et al., 2018).

CONCLUSIONS

The paper briefly described the methodology and shows the preliminary results of the processing that was performed on the passive seismic data collected during 14 days in October 2017. As very little injection tests were performed until this period, this dataset can be used as baseline reference for further studies. We show some examples of continuous seismic data and associated spectrograms. One punctual event we can detect in the continuous signal are due to the Vibroseis truck used for active survey during the recording period. We can also detect others punctual events repeating themselves over the 14 days which origin needs to be investigated. Further analysis using match-field processing will be used on this dataset to see if we can detect any presence of baseline microseismicity.

Processing and correlation computation were done using the Python Code MSNoise (Lecocq et al., 2014). Resulting correlations shows asymmetric signal which will be further investigate to study noise directivity. However, correlation shows good emergence of the surface wave which allows the computation of group velocity dispersion curves showing values coherent with expectation.

Finally, we start to look at the stability in the correlations for that baseline dataset and they show good stability over time. We compute the $\delta v/v$ for a selection of station pairs. They show very low velocity variations ($\pm$ 0.1%) with a general decreasing velocity. Further investigation needs to be done to analyze this result.

ACKNOWLEDGEMENTS

We thank CaMI JIP and CREWES sponsors for their financial support. We also gratefully acknowledge support from NSERC (Natural Science and Engineering Research Council of Canada) through the grant CRDPJ 461179-13. This research was undertaken thanks in part to funding from the Canada First Research Excellence Fund. We thank Thomas Lecocq for developing and distributing the MSNoise codes.

REFERENCES

Arts, R., Chadwick, A., Eiken, O., Thibeau, S., and Nooner, S., 2008, Ten years' experience of monitoring CO_2 injection in the Utsira Sand at Sleipner, offshore Norway: First break special topic CO_2 sequestration, **26**.

Bensen, G. D., Ritzwoller, M. H., Barmin, M. P., Levshin, A. L., Li, F., Moschetti, M. P., Shapiro, N. M., and Yang, Y., 2007, Processing seismic ambient noise data to obtain reliable broad-band surface wave dispersion measurements: Geophysical Journal Internationa, **169**, 1239–1260.

Bergmann, P., Ivandic, M., Norden, B., Rücker, C., Kiessling, D., S., S. L., Schmidt-Hattenberger, C., and Juhlin, C., 2013, Combination of seismic reflection and constrained resistivity inversion with an application to 4d imaging of the CO_2 storage site, Ketzin, Germany: Geophysics, **79**, No. 2, B37–B50.

Boullenger, B., Verdel, A., Paap, B., Thorbecke, J., and Draganov, D., 2015, Studying CO_2 storage with ambient-noise seismic interferometry: A combined numerical feasibility study and field-data example for ketzin, germany: Geophysics, **80**, No. 1.

Brenguier, F., Rivet, D., Obermann, A., Nakata, N., Boué, P., Lecocq, T., Campillo, M., and Shapiro, N., 2016, 4-d noise-based seismology at volcanoes: Ongoing efforts and perspectives: Journal of Volcanology and Geothermal Research, **321**, 182–195.

Campillo, M., and Paul, A., 2003, Long-range correlations in the diffuse seismic coda: Science, **299**, No. 5606, 547–549.

Clarke, D., Zaccarelli, L., Shapiro, N., and Brenguier, F., 2011, Assessment of resolution and accuracy of the moving window cross spectral technique for monitoring crustal temporal variations using ambient seismic noise: Geophysical Journal International, **186**, No. 2, 867–882.

Delatre, M., and Manceau, J.-C., 2013, Applicability of long-range seismic noise correlation for CO_2 geological storage monitoring: Energy Procedia, **37**, 4049–4056.

Duputel, Z., Ferrazzini, V., Brenguier, F., Shapiro, N., Campillo, M., and Nercessian, A., 2009, Real time monitoring of relative velocity changes using ambient seismic noise at the piton de la fournaise volcano (la Réunion) from january 2006 to june 2007: Journal of Volcanology and Geothermal Research, **184**, 164–173.

Gassenmeier, M., Sens-Schönfelder, C., Delatre, M., and Korn, M., 2014, Monitoring of environmental influences on seismic velocity at the geological storage site for CO_2 in Ketzin (Germany) with ambient seismic noise: Geophysical Journal International, **200**, No. 1, 524–533.

Gordon, A., and Lawton, D. C., 2017, Zero offset VSP processing of fiber optic cable (DAS) and geophone array at the CaMI Field Research Station: CREWES Research Report, **29**.

Gordon, A., and Lawton, D. C., 2018, Walk away VSP processing of DAS and geophone data at the CaMI Field Research Station, Newell county, Alberta: CREWES Research Report, **this volume**.

Gordon, A., Lawton, D. C., and Eaton, D. W., 2016, VSP azimuthal travel time analysis at the Field Research Station near Brooks, Alberta: CREWES Research Report, **28**.

Hadziioannou, C., Larose, E., Coutant, O., Roux, P., and Campillo, M., 2009, Stability of monitoring weak changes in multiply scattering media with ambient noise correlation: Laboratory experiments: The Journal of the Acoustical Society of America, **125**, No. 6, 3688–3695.

Hall, K. W., Bertram, K., Bertram, M., Innanen, K., and Lawton, D., 2018, Crewes 2018 multi-azimuth walk-away VSP field experiment: CREWES Research Report, **this volume**.

Hall, K. W., Isaac, J. H., Wong, J., Bertram, K. L., Bertram, M. B., Lawton, D. C., Bao, X., and Eaton, D., 2015, Initial 3C-2D surface seismic and walkaway VSP results from the 2015 Brooks SuperCable experiment: CREWES Research Report, **27**.

Hall, K. W., Lawton, D. C., Daley, T., Freifeld, B., and Cook, P., 2017, Source distance and source effort on DAS data: CREWES Research Report, **29**.

Herrmann, R. B., 2013, Computer programs in seismology: An evolving tool for instruction and research: Seismological Research Letters, **84**, No. 6, 1081–1088.

Isaac, J. H., and Lawton, D. C., 2015, 3D3C seismic data at the Brooks experimental CO_2 injection site: CREWES Research Report, **27**.

Isaac, J. H., and Lawton, D. C., 2017, A summary of surface seismic reflection data acquired at the field research station near brooks, alberta: CREWES Research Report, **29**.

Lawton, D. C., Bertram, M., Bertram, K., Hall, K., and Isaac, H., 2015a, A 3C-3D seismic survey at a new field research station near Brooks, Alberta: CREWES Research Report, **27**.

Lawton, D. C., Bertram, M., and Bertram, K. H. K., 2015b, New approaches to seismic monitoring at the Brooks Field Research Station: CREWES Research Report, **27**.

Lawton, D. C., Bertram, M. B., Saeedfar, A., and Macquet, M., 2017, DAS installations at the CaMI Field Research Station: CREWES Research Report, **29**.

Lecocq, T., Caudron, C., and Brenguier, F., 2014, MSNoise, a Python package for monitoring seismic velocity changes using ambient seismic noise: Seismological Research Letters, **85**, No. 3, 715–726.

Levshin, A., Yanocskaya, T. B., Lander, A. V., Bukchin, B. G., Barmin, M. P., Ratnikova, L. I., and Its, E. N., 1989, Seismic surface waves in a laterally inhomogeneous earth: edited by V. I. Keilis-Borok, Springer, New York.

Mac Dowell, N., Fennell, P., Shah, N., and Maitland, G., 2017, The role of CO_2 capture and utilization in mitigating climate change: Nature Climate Change, 7/243.

Macquet, M., Paul, A., Pedersen, H., Villaseñor, A., Chevrot, S., Sylvander, M., and Wolyniec, D., 2014, Ambient noise tomography of the Pyrenees and the surrounding regions: inversion for a 3-D Vs model in the presence of a very heterogeneous crust: Geophysical Journal International, **199**, No. 1, 402–415.

Mainsant, G., Larose, E., Brönnimann, C., Jongmans, D., Michoud, C., and Jaboyedoff, M., 2012, Ambient seismic noise monitoring of a clay landslide: Toward failure prediction: Journal of Geophysical Research: Earth Surface, **117**, No. F1.

Mordret, A., Landès, M., Shapiro, N., Singh, S., and Roux, P., 2014, Ambient noise surface wave tomography to determine the shallow shear velocity structure at Valhall: depth inversion with a neighbourhood algorithm: Geophysical Journal International, **198**, No. 3, 1514–1525.

Obermann, A., Kraft, T., Larose, E., and Wiemer, S., 2015, Potential of ambient seismic noise techniques to monitor the St. Gallen geothermal site (Switzerland): Journal of Geophysical Research: Solid Earth.

Olivier, G., Chmiel, M., Brenguier, F., Roux, P., Mordret, A., Dales, P., Lecocq, T., Djamaludin, I., and Dodds, K., 2018, Processing passive seismic data recorded on a dense array for CCS site characterization: SEG International Exposition and 88th Annual Meeting.

Ratdomopurbo, A., and Poupinet, G., 1995, Monitoring a temporal change of seismic velocity in a volcano: Application to the 1992 eruption of Mt. Merapi (Indonesia): Geophysical research letters, **22**, No. 7, 775–778.

Rostron, B., White, D., Hawkes, C., and Chalaturnyk, R., 2014, Characterization of the aquistore CO_2 project storage site, Saskatchewan, Canada: Energy Procedia.

Shapiro, N., and Campillo, M., 2004, Emergence of broadband Rayleigh waves from correlations of the ambient seismic noise: Geophysical Research Letters, **31**, No. 7.

Shapiro, N. M., Campillo, M., Stehly, L., and Ritzwoller, M. H., 2005, High-resolution surface-wave tomography from ambient seismic noise: Science, **307**, No. 5715, 1615–1618.

Spackman, T. W., and Lawton, D. C., 2017, Seismic monitoring with continuous seismic sources: CREWES Research Report, **29**.

Spackman, T. W., and Lawton, D. C., 2018, Processing and analysis of data recorded from a buried permanent seismic source: CREWES Research Report, **this volume**.

Stehly, L., Fry, B., Campillo, M., Shapiro, N., Guilbert, J., Boschi, L., and Giardini, D., 2009, Tomography of the Alpine region from observations of seismic ambient noise: Geophysical Journal International, **178**, No. 1, 338–350.

Storke, A., Allmarkb, C., Curtis, A., Kendall, J., and White, D., 2018, Assessing the potential to use repeated ambient noise seismic tomography to detect CO_2 leaks: Application to the Aquistore storage site: International Journal of Greenhouse Gas Control, **71**.